PCCP

Accepted Manuscript

ROYAL SOCIETY OF CHEMISTRY

www.rsc.org/pccp

Cite this: DOI: 10.1039/c0xx00000x

www.rsc.org/xxxxxx

PAPER

Organic nanoparticles of malachite green with enhanced far-red emission: Size-dependence of particle rigidity

Tomohito Funada,[a] Takuya Hirose,[b] Naoto Tamai[b] and Hiroshi Yao*[a]

Received (in XXX, XXX) Xth XXXXXXXXX 200X, Accepted Xth XXXXXXXXX 200X

DOI: 10.1039/b000000x

In tracing the biological processes by fluorescent probes, it is desirable to shift the excitation/emission energy to far-red/near-infrared (FR/NIR) region. In this study, we successfully synthesize FR fluorescent organic nanoparticles via ion-association between malachite green (MG) cation and tetrakis(4-fluorophenyl)borate (TFPB) anion in the presence of a neutral stabilizing polymer. Binding of MG with TFPB results in the prominent appearance of an absorption band that can be assigned to an H-aggregate of MG. The fluorescence intensity as well as the fluorescence lifetime show a significant increase with a decrease in the nanoparticle size. Since the MG dye is known as a local viscosity or environmental rigidity probe showing a rotational friction dependence of the excited state lifetime, we find that rigidity of the organic nanoparticle is strongly size-dependent; that is, the smaller the size of the nanoparticle, the greater the rigidity in the nanoparticle. We also reveal that surface regions of the ion-based organic nanoparticles are more rigid than inside. The presence of H-aggregates that are almost non-fluorescent is the major origin of aggregation-caused quenching (ACQ) and still avoids enhancing the fluorescence quantum yield of the MG nanoparticles, so we develop a new approach to prevent H-aggregation inside the nanoparticle by incorporating photochemically inert, bulky phosphonium cations, which results in a 430-fold enhancement of its fluorescence yield. We believe such methodology will open an avenue in the development of new types of fluorescent nanomaterials for many applications.

Introduction

Spectrofluorimetry in the far-red/near-infrared (FR/NIR) region (~650–1000 nm) is an important research field; for example, in the cell tracing, it is desirable to shift the excitation and emission to longer FR/NIR wavelengths, which will avoid photo-damage caused by UV-vis high-energy excitation, achieve deep tissue penetration, and reduce the spectral overlap with cell-based autofluorescence.[1] Such FR/NIR energy region is typically called "biological window",[2] and there is potential for the development of a noninvasive clinical diagnostic.[3–5] Accordingly, the development of FR/NIR fluorophores for such applications has been receiving strong attention.[6–8] Then a number of FR/NIR-emissive materials, particularly nanomaterials, have been exploited, which include quantum dots,[9] fluorescent proteins,[10] and metal nanoclusters/nanoshells.[11] In this regard, improvement of photophysical properties in the nanomaterials such as high molar extinction coefficient, high fluorescence quantum yield and thermal/chemical stability is still actively sought.

Malachite green (MG), one of triphenylmethane dyes, is a far-red (but almost non-fluorescent) organic dye that has been used to generate fluorescent signal when bound specifically to selected proteins such as fluorogen activating proteins (FAPs) or nucleic acid aptamers.[12,13] The photoluminescent properties of the MG dye can be then suited to fluorescent nanoprobes in the biological window range if molecular aggregation through π–π stacking interaction is avoided (and thus almost no aggregation-caused quenching (ACQ) deexcitation is achieved), because conventional FR/NIR fluorophores are normally large π-functional planar molecules that can frequently induce ACQ in the aggregate state.[14] Moreover, in the excited state dynamics of MG in fluid media, the first singlet state (S_1) is known to undergo ultrafast nonradiative relaxation, and its lifetime (and resultant fluorescence quantum yield) strongly depends on the medium viscosity due to strong coupling between electronic states and the torsional degrees of freedom;[15–19] that is, the relaxation of MG is intrinsically barrierless and involves rotation of the phenyl substituents, so the friction exerted by the environment on the rotating rings accounts for the viscosity dependence of the excited state lifetime.[15–19] Hence the fluorescence lifetimes have been found to be proportional to the viscosity (η) raised to a power ranging roughly between 0.33 and 1.0.[16–21] Note that the lifetime is almost independent on the solvent polarity.[20,21] Although, for example, it is not clear what is the exact nature of the intermediate state in the relaxation pathway, the MG dye can be used as a local viscosity or rigidity probe.

On the basis of the above considerations, the radiative lifetimes and/or fluorescence quantum yields of MG will be enhanced substantially upon binding of MG with hydrophobic counteranions such as phenylborate derivatives to form ion-based organic nanoparticles.[22] Such ion-based organic nanoparticles

have been synthesized on the basis of the formation of water-insoluble ion-pair solids in aqueous phases by association of a chromophoric ion with a hydrophobic (non-chromophoric) counterion.[23–25] In the present study, preparation of organic nanoparticles of MG with enhance far-red fluorescence via the ion-association approach is reported. Ion-pair (or electrostatic) interaction and subsequent incorporation of MG in the nanoparticle can bring about rigidification of phenyl rings (or restriction of intramolecular rotation) in the dye molecule. As expected, enhancement of the fluorescence quantum yield and fluorescence lifetime of MG is observed upon formation of the MG nanoparticles. Interestingly, rotational motion or diffusion of phenyl rings of MG in the solid-state nanoparticles is strongly particle size dependent; that is, it is still fast when the size of nanoparticles is large, and the smaller the size is, the greater the rigidity of the nanoparticles becomes. In addition, formation of almost non-fluorescent H-aggregates of MG in the nanoparticles is found to discourage some FR fluorescence, but we overcome this problem by incorporating foreign photochemically-inert tetraphenylphosphonium cations in the MG nanoparticles to reduce ACQ. Consequently, we show that MG nanoparticles indeed increases the FR fluorescence ~430-fold stronger than that in water.

Experimental

Materials

Malachite green (MG; chemical structure is shown in Fig. 1a) oxalate (99.4%) was purchased from Wako Pure Chemical Industries and used as received. Poly(vinylpyrrolidone) (PVP; average M_W = 10000, Aldrich) was used as a neutral stabilizer to prevent particle agglomeration. Sodium tetrakis(4-fluorophenyl)borate dihydrate ($NaTFPB•2H_2O$, Aldrich; see also Fig. 1a) and tetraphenylphosphonium chloride (TPPhosCl, Aldrich; see Fig. 3) were of the highest commercial grade available and used as received without further purification. Pure water was obtained by an Advantec GS-200 automatic water-distillation supplier.

Synthesis

Organic MG nanoparticles. Organic MG nanoparticles were prepared by means of the ion-association method.[22–25] Typically, rapid addition of aqueous TFPB solution (0.1 mM; 1–2 mL) containing PVP into ultrasonicated aqueous solution of native MG dye (0.05 mM; 1–2 mL), at the molar ratio (ρ = [TFPB]/[MG]) changing from 1 to 4, produced almost clear greenish suspension. The pH of the solutions of these MG nanoparticle samples was 4.8–5.1. The concentration of PVP was set at 0.4 mg/mL. The characteristic Tyndall scattering gave confirmatory evidence that ion-association between cationic MG^+ and anionic $TFPB^-$ led to the formation of water-insoluble MG nanoparticles. Note that, in the absence of PVP, the preparation procedures at ρ = 1 or 4 also gave stable solid-state particles showing strong Tyndall scattering in solution, so we also evaluated these particles in a similar manner to those prepared in the presence of PVP. The solution-phase stability of synthesized MG nanoparticles was also analyzed by taking into account the time evolution of their absorption spectra. See the ESI†. The procedure of keeping the samples for a week under dark at room temperature resulted in a little change in their UV-vis absorption.

Prevention of ACQ by phosphonium doping into the MG nanoparticles. To prevent aggregation-caused quenching (ACQ) that was observable in the MG nanoparticles, we tried dilution of MG concentration inside the nanoparticles by co-incorporating (or mixing) the photochemically-inert hydrophobic tetraphenylphosphonium (TPPhos) cations. In other words, the purpose of inclusion of TPPhos inside the MG nanoparticles is to avoid formation of almost non-fluorescent MG H-aggregates. The TPPhos cations can also interact with TFPB anions electrostatically, which interferes aggregation of MG molecules in the nanoparticles. The TPPhos-mixed MG nanoparticles were prepared by the ion-association protocol for the binary cation mixtures (MG and TPPhos) and anionic TFPB under the condition of ρ = 4, in the presence of PVP ([PVP] = 0.4 mg/mL), in aqueous solution. The mixing ratio (molar fraction) of MG and TPPhos ([TPPhos]/[MG]) was changed to 1 or 5, but the total cation concentration (= [MG] + [TPPhos]) did not alter. The pH of these sample solutions was 5.4–5.7. In addition, the system stability of these sample solutions was also examined by time evolution of UV-vis absorption spectra (See also the ESI†).

Instrumentation

Morphology and size of the nanoparticles were examined with a Hitachi S-4800 scanning transmission electron microscope (STEM). A specimen for STEM observations was prepared by dropping the suspension on an amorphous carbon-coated copper mesh. UV-vis absorption spectra were recorded on a Hitachi U-4100 spectrophotometer. Fluorescence spectra were obtained with a Hitachi F-4500 spectrofluorometer. Fluorescence quantum yields (Φ_f) were determined by comparing the emission spectra of DTDCI (3,3'-diethylthiadicarbocyanine iodide) in methanol (Φ_f = 0.32).[26] Fluorescence lifetime measurements were carried out with a time-correlated single-photon counting system.[27] The second harmonic of the output from a mode-locked femtoseocnd Ti:sapphire laser (Spectra Physics, Tsunami) was used for excitation (410 nm). The repetition rate was reduced with a pulse picker. Fluorescence from the sample at 680 nm was obtained with a monochromator (Japan Spectroscopic, CT-10) and detected with a photomultiplier system.[27] The procedure for the fluorescence lifetime analysis was an iterative reconvolution, so lifetimes down to a factor of 0.1–0.15 of the IRF (Instrument Response Function) width can be recovered.[28,29] Spectroscopic (steady-state and time-resolved) measurements were conducted at room temperature.

Results and discussion

Spectroscopic properties of MG nanoparticles

A series of organic MG nanoparticles dispersed in aqueous solution were successfully synthesized, which could be confirmed by their characteristic Tyndall scattering (Fig. 1a). Fig. 1b shows UV-vis absorption spectra of MG nanoparticle samples prepared at ρ = 1, 2 and 4, along with that of native MG in water. The absorption of MG in water shows two peaks, one at 425 nm corresponding to the monomer transition polarized to the *y*-axis and other (major peak) at 617 nm corresponding to that polarized to the *x*-axis (see also Fig. 1a). In comparison with the absorption

spectrum of MG in water, the monomer peak was red-shifted to around 628 nm for the nanoparticle samples, indicating that MG was bound to TFPB to produce ion-pair species.[22,30] The most significant feature is the observation of a prominent peak at higher energy (~596 nm). This peak can be attributed to an H-type aggregate of MG including H-dimers.[31,32] Additionally, with an increase in ρ, the absorbance ratio of A_H/A_M, where the suffix H or M represents the H-aggregate (monitored at 596 nm) or monomer (monitored at 628 nm), respectively, increased slightly; A_H/A_M = 0.90, 0.93, and 0.94 for ρ = 1, 2, and 4, respectively. This behavior is similar to that observed for ion-pair-based cyanine dye nanoparticles.[23–25]

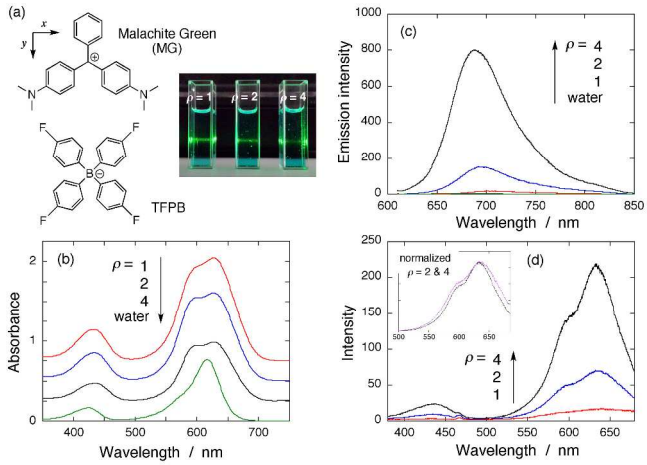

Fig. 1. (a) Chemical structures of malachite green (MG) cation and tetrakis(4-fluorophenyl)borate (TFPB) anion. A photo of Tyndall scattering taken under green laser irradiation is also shown. (b) Absorption spectra of MG nanoparticles prepared at the molar ratio (ρ) of 1, 2, and 4, together with that of liberated MG dye in aqueous solution. The molar ratio ρ is defined as [TFPB]/[MG]. Spectra are offset by a constant (absorbance 0.25 each) for clarity. (c) Fluorescence spectra of MG nanoparticle samples prepared at ρ = 1, 2, and 4, along with that of liberated MG dye in aqueous solution (λ_{ex} = 600 nm). (d) Excitation spectra of MG nanoparticle samples (λ_{em} = 700 nm). For the measurements, samples were diluted to avoid spectral distortion.

A series of fluorescence spectra of the MG nanoparticle samples are shown in Fig. 1c, together with the fluorescence of native MG in water (λ_{ex} = 600 nm). It is worth noting here that these nanoparticles display emission peaks in the FR/NIR region of the "biological window" (650-1000 nm), which may be advantageous for imaging purposes in biological studies. The fluorescence of aqueous MG solution was very weak ($\Phi_f = 7.9 \times 10^{-5}$); however, upon formation of nanoparticles via ion-association, a substantially enhanced fluorescence intensity was found. Of particular interest is that as the ρ value increases, the fluorescence becomes more intense. For example, fluorescence of MG nanoparticles prepared at ρ = 4 has the intensity with ~160-fold enhancement compared to that of native MG in water. Note that this enhancement factor is just an approximation since the absorbance correction was not conducted. To more quantitatively estimate the fluorescence quantum yields (Φ_f) of the MG nanoparticles, all samples were diluted with water appropriately, and the fluorescence yields were determined as follows;[26] Φ_f = ~4.5×10^{-4} (ρ = 1), ~4.0×10^{-3} (ρ = 2), and ~1.5×10^{-2} (ρ = 4). It is known that MG dye has an extremely low quantum yield for fluorescence due to easy vibrational or rotational deexcitation, but viscous or rigid environments encourage fluorescence by restricting such vibrations or rotational diffusion.[15–21] Hence a range of conformations over which the dye will experience twisting through the angle of deexcitation is prevented by binding with TFPB counteranions, keeping the more fluorescent conformation stabilized in the nanoparticles.[15]

Fig. 1d shows excitation spectra of a series of MG nanoparticle samples (λ_{em} = 700 nm). All excitation spectra are essentially similar to the absorption spectrum of MG monomer, suggesting that monomeric MG species in the nanoparticles can only emit intense fluorescence. In other words, MG H-aggregates produced in the nanoparticles, which were obviously detected in the absorption spectra, are non-fluorescent, so to further enhance the FR/NIR emission from the nanoparticles, suppression or prevention of formation of the non-fluorescent H-aggregates should be significant.

Particle sizes

Fig. 2 shows typical results on STEM observations of the MG nanoparticles prepared at ρ = 1, 2, and 4. The STEM images reveal that the samples have the particle diameters in the range of 30–90 nm (ρ = 1), 20–40 nm (ρ = 2), and 10–30 nm (ρ = 4). The size distributions are obtained directly from STEM photographs, and shown also in Fig. 2. The mean diameter of nanoparticles are 45.6, 23.6, and 14.3 nm for the ρ = 1, 2, and 4 samples, respectively. We found that, as the ρ increases, the particle size decreases and thereby the dispersion is reduced. This behavior is very similar to that observed for various kinds of cyanine dye nanoparticles synthesized in the same ion-based manner.[23–25] The increase in surface adsorption of TFPB can bring about the reduction of the surface tension of nanoparticles according to the Gibbs' adsorption equation,[22] resulting in the decrease in particle size. Note that, on the basis of the size of the MG-TFPB ion-pair adduct, which could be calculated by quantum chemical calculations, the average number of MG molecules in a signle nanoparticle can be estimated as about 2900, 400, and 90 for the ρ = 1, 2, and 4 nanoparticle samples, respectively. See the ESI† for more detail.

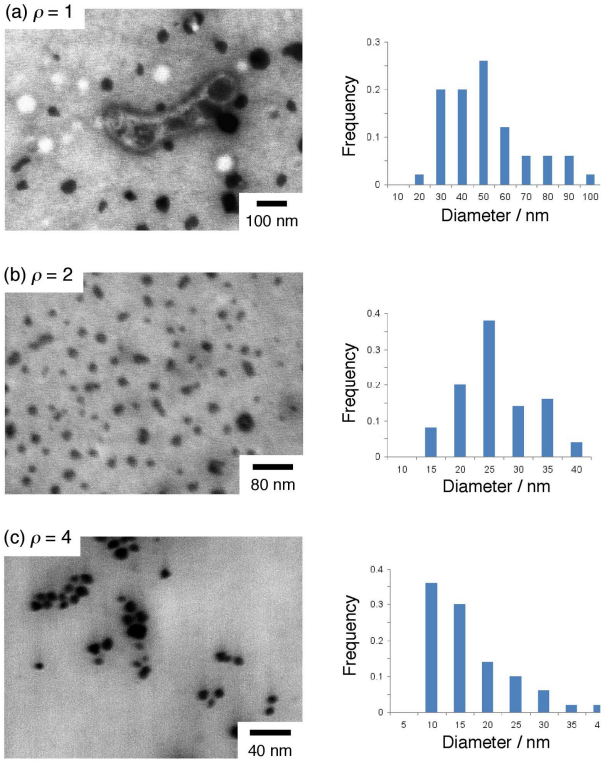

Fig. 2. (a)–(c) STEM images and the corresponding particle size distributions of the MG nanoparticle samples prepared at ρ = 1, 2 and 4, respectively.

Suppression of ACQ: Additional fluorescence enhancement

As described before, fabrication of highly fluorescent organic nanoparticles with emission in the FR/NIR region and their excellent stability is envisaged.[3–14] In the present case, realization requires prevention of non-fluorescent (or weakly-fluorescent) H-aggregate formation of MG dye in the solid-state nanoparticles (a general phenomenon known as ACQ). To minimize or eliminate the formation of MG H-aggregates in the nanoparticle, we tried to remove stacking interactions between the MG molecules in course of the nanoparticle formation by co-doping of bulky phosphonium (TPPhos) cations having photochemically inert and hydrophobic nature. This methodology can make the MG concentration (or content) in a particle decrease and thus prevent H-aggregation between the MG chromophores.

Fig. 3a or 3b displays a typical STEM image of the TPPhos-incorporated MG nanoparticle sample prepared at ρ = 4 with the mixing molar ratio ([TPPhos]/[MG]) of 1 or 5 (that is, TPPhos incorporation level of 50% or 83.3%), respectively. Size distributions are also shown in the figure. From Fig. 3, the particle sizes were still in the range of 10–40 nm, and the mean diameter was obtained to be 16.2 or 14.2 nm for the sample with the incorporation level of 50 or 83.3%, respectively. This means that the particle size was *not* influenced by incorporation of cationic TPPhos under the present conditions; that is, the size of the nanoparticles should be determined by the overall ρ value, not by the concentration (or fraction) of cationic MG and TPPhos. This is probably due to the fact that, in the present system, molecular dimension of TPPhos is similar to that of MG or TFPB, so it is expected that TPPhos cations are uniformly distributed in the nanoparticle.

Fig. 4a shows UV-vis absorption spectra of TPPhos-incorporated MG nanoparticle samples prepared at ρ = 4, with the mixing molar ratios of [TPPhos]/[MG] = 0, 1, and 5 (or incorporation level of 0%, 50%, or 83.3%, respectively). The effect of TPPhos incorporation is remarkable, that is, the H-band becomes significantly reduced with increasing the incorporation level of TPPhos, which proves less π-π stacking interactions and H-aggregate formation of MG molecules. Namely, the TPPhos plays a important role in distancing two or more MG molecules from each other. Fig. 4b displays fluorescence spectra of the resultant *ACQ-suppressed* MG nanoparticles. Despite a lower optical density for the TPPhos-incorporated MG nanoparticles, the fluorescence intensity was almost unchanged. We then estimated fluorescence quantum yields for these nanoparticle samples through appropriate dilution and subsequent absorbance normalization; they are $\Phi_f = 1.7 \times 10^{-2}$ (incorporation level; 50%) and $\Phi_f = 3.4 \times 10^{-2}$ (incorporation level; 83.3%). Upon incorporation of TPPhos, consequently, we found that the fluorescence from *ACQ-suppressed* MG nanoparticles was ~430 times greater than that of liberated MG in water.

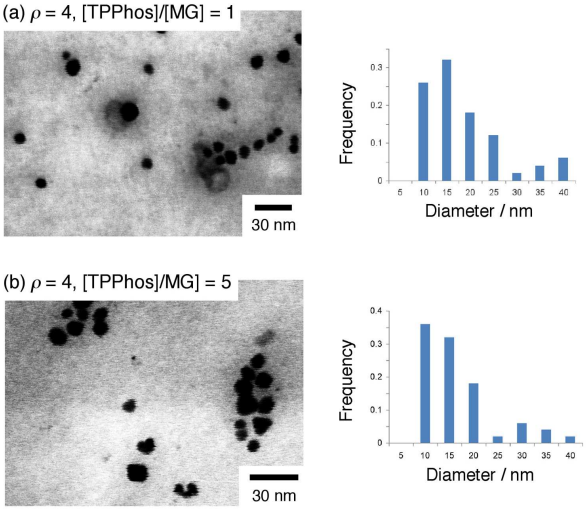

Fig. 3. (a) and (b) STEM images and the corresponding particle size distributions of the *ACQ-suppressed* MG nanoparticle samples prepared with the dopant mixing ratio [TPPhos]/[MG] of 1 and 5, respectively, under the condition of ρ = 4.

Interestingly, in the presence of foreign TPPhos dopant, a bathochromic shift of ~7 nm was observed for the MG monomer absorption band but the fluorescence peak position was shifted to blue, bringing about smaller Stokes shift compared to the samples without TPPhos doping. The observed bathochromic shift of the monomer position probably indicates the solvent (TPPhos/TFPB mixed-matrix) effect. On the other hand, the smaller Stokes shift suggests that relaxation of the photoexcited MG dye through geometrical alternation is smaller, as expected for the behavior in more-confined environment.[33] Hence an increase in the rigidity around MG would also cause additional emission enhancement. Fig. 4c shows excitation spectra for the ACQ-suppressed MG nanoparticles. Upon incorporation of TPPhos, the spectral linewidth of the MG monomer band became narrow, strongly indicating that the fluorescence state of MG dye is readily subject to inhomogeneous broadening, and stochastic fluctuations or

conformational heterogeneity can be reduced by the addition of TPPhos into the nanoparticles.[25]

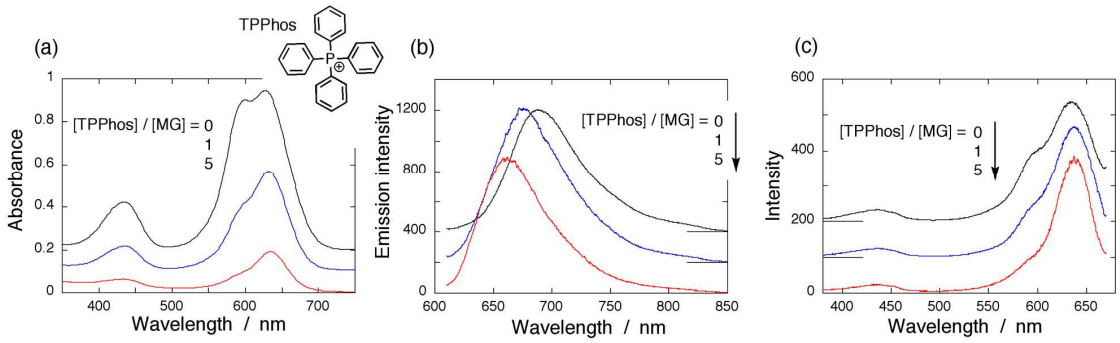

Fig. 4. (a)–(c) Absorption, fluorescence, and excitation spectra of ACQ-suppressed MG nanoparticles prepared at the mixing ratio [TPPhos]/[MG] of 0, 1, and 5, respectively, under the condition of $\rho = 4$. All spectra are offset by a constant (absorbance; 0.1 each, emission; 200 each, and excitation; 100 each) for clarity. Note that chemical structure of tetraphenylphosphonium cation (TPPhos) is also shown in the inset (a).

Picosecond fluorescence dynamics

The fluorescence quantum yield and/or fluorescence lifetime of MG are strongly dependent on the medium viscosity;[15–19,34] in non-viscous solvents, the nonradiative relaxation process of MG occurs very rapidly, but in viscous solvents, the fluorescence lifetime becomes considerably long. Hence to evaluate the local viscosity (in the present case, "*particle rigidity*" would be more appropriate) around MG molecules in the nanoparticles and the related relaxation pathways of S_1 states of the dye, fluorescence lifetime measurements were carried out for a series of the nanoparticles with different particle sizes (= ρ values) and different incorporation levels of TPPhos. Note that MG has a very fast fluorescence lifetime of shorter than ~1 ps in water,[28,35] so to avoid wavelength-dependent uncertainty of the IRF, and to directly compare the fluorescence lifetimes between the solution-phase and nanoparticle samples, all decay curves were analyzed by using that of MG in water (monitored at 680 nm) as the IRF (The fluorescence decay curve of MG in water is displayed in the ESI†). The fluorescence transients are shown in Fig. 5. All decay curves were successfully fitted with bi- or tri-exponential function; in a tri-exponential fit, $A_1\exp(-t/\tau_1) + A_2\exp(-t/\tau_2) + A_3\exp(-t/\tau_3)$ is applied, where A_i is the pre-exponential factor for the *i*-th component and τ_i is the corresponding fluorescence lifetime. The present analysis with a sum of two or three exponentials is a common and similar procedure with that for the fluorescence of MG in the polymer matrices.[28,34] In addition, the average lifetime τ_{av} was defined as $\tau_{av} = A_1\tau_1 + A_2\tau_2 + A_3\tau_3$. The obtained kinetic parameters of various MG nanoparticles are tabulated in Table 1.‡ The time constant can be essentially ascribed to the relaxation from the S_1 state to the nonradiative intermediate state (often referred to as S_x) that involves a rotation of (substituted and/or non-substituted) phenyl rings, followed by very fast deexcitation to the ground state through a twist-back, flattening the structure of the molecule.[36–38] The resulting highly torsional conformation in the electronic ground state is related to the intermediate state S_x (or conical intersection), and thus the fluorescence lifetime (precisely, nonradiative decay rate) shows a strong dependence on the particle rigidity (see Fig. 6; a schematic energy diagram of MG explaining the excited-state deactivation pathway that is dependent on the rigidity of the medium).[36–38] In other words, the increase in the average fluorescence lifetime is attributed to that in the motional rigidity or restricted rotation of phenyl rings in MG.

Table 1. Kinetic parameters of relaxation dynamics (fluorescence lifetimes) of a series of malachite green (MG) nanoparticles. The fluorescence decay profile could be fitted with tri-exponential (or bi-exponential) function.

sample	comment	A_1	τ_1 (ps)	A_2	τ_2 (ps)	A_3	τ_3 (ns)	τ_{av} (ps)
$\rho = 1$		0.984	17	0.016	157	——	——	19
$\rho = 2$		0.884	28	0.094	297	0.022	2.12	53
$\rho = 4$	[TPPhos] / [TFPB] = 0	0.544	78	0.314	500	0.142	2.54	200
	[TPPhos] / [TFPB] = 1	0.568	83	0.300	516	0.132	2.52	202
	[TPPhos] / [TFPB] = 5	0.532	103	0.311	574	0.156	2.63	234
$\rho = 1$	no PVP	0.976	≤ 8 (3)	0.024	31	——	——	≤ ~8 (3.7)
$\rho = 4$	no PVP	0.874	7	0.111	21	0.015	0.087	8

For the MG nanoparticles, strikingly, the average fluorescence lifetime shows a strong dependence on the particle size; with an increase in ρ, or with decreasing the size of the nanoparticles, an increase in the average decay time is obvious (τ_{av} = 53 and 200 ps for ρ = 2 and 4, respectively). This can be attributed to the increase in the rigidity around MG in the nanoparticle, which causes a slow down of the nonradiative decay; that is, surprisingly, the *smaller* nanoparticles have *greater* particle rigidity inside.§ Indeed, an increase in the fluorescence lifetime corresponds to that in the fluorescence quantum yield of the nanoparticles. In contrast, incorporation of TPPhos did not contribute to the extension of the average fluorescence lifetime (τ_{av} = 202 and 234 ps for the incorporation level of 50 and 83.3% (ρ = 4), respectively), but to the enhancement of the fluorescence quantum yield (see also Table 1). This is in reasonable agreement with the fact that MG H-aggregates produced in the nanoparticle are non-fluorescent, and the methodology using photochemically-inert ionic dopant, which suppresses the dye H-aggregate formation, is significant for obtaining highly fluorescent organic nanoparticles.

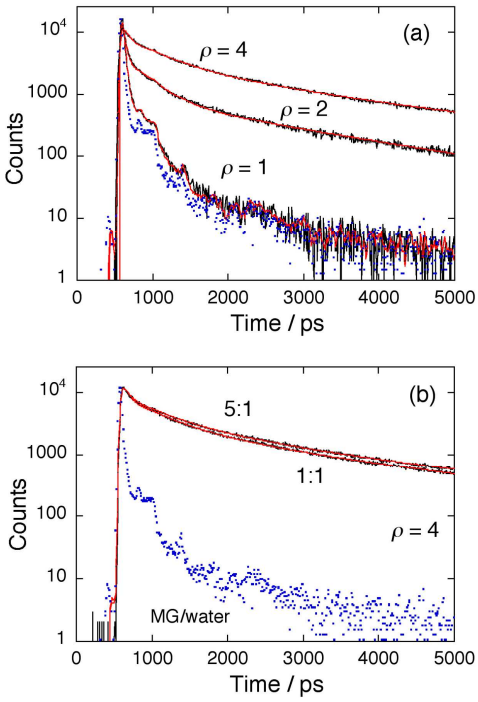

Fig. 5. (Black curve) Fluorescence decay curves of (a) MG nanoparticles prepared at $\rho = 1$, 2, and 4, in aqueous solution, and (b) ACQ-suppressed MG nanoparticles with the dopant mixing ratio of 1 and 5. Excitation wavelength is tuned to 410 nm. Fluorescence emission is collected at 700 nm. (Red curve) Decay fits by tri-exponential functions. (Blue dot) IRF; instrument response function. We used the fluorescence decay curve of MG in water as the IRF.

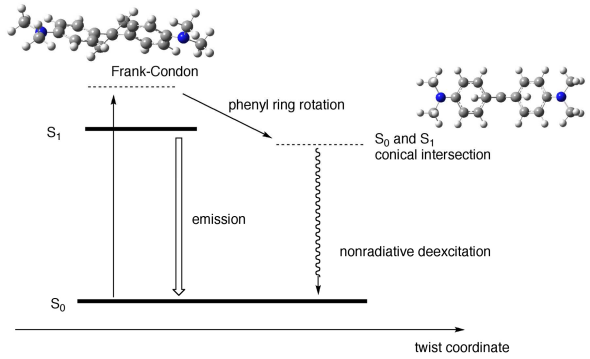

Fig. 6. Typical ground- and excited-state energy diagram of MG dye, and the excited-state deactivation pathway explaining the medium rigidity dependence of the non-radiative decay rate by the twisted character of the phenyl substituents in MG.

MG Nanoparticles Synthesized in the absence of PVP

We also found that the MG nanoparticle system prepared in the *absence* of the stabilizing polymer PVP tends to form almost no flocculates, so the effect of surface-adsorbed PVP on their spectroscopic properties was examined. The organic MG nanoparticles were then prepared at $\rho = 1$ and 4, without using PVP, in a similar ion-based manner. The results (absorption and fluorescence spectra, fluorescence decay curves, and size data based on the STEM observations) are summarized in Fig. 7. Fluorescence lifetimes obtained are also listed in Table 1. Firstly, the diameters are in the range of 40–60 nm for the sample with $\rho = 1$ and 50–80 nm for that with $\rho = 4$. The particle diameters are similar to each other; however, in comparison with those prepared in the *presence* of PVP, the particles were generally larger and easier to flocculate in a certain case (see Fig. 7e), suggesting that PVP has a distinct influence on stabilization of the organic nanoparticles. Note here that excess TFPB anion obviously plays a role in stabilizing ion-based MG nanoparticles probably because of its surface adsorption giving effective surface charges (see Fig. 7f).[22] Secondly, we observed both monomer and H-bands of MG in the absorption spectra, which were very similar to those of the nanoparticle system prepared in the presence of PVP. In contrast, enhancement in the fluorescence intensity and its lifetime was marginal, and their fluorescence quantum yields were ~10^{-4}. Note that aqueous (liberated) MG solution in the presence of PVP still exhibited very weak fluorescence (almost no enhancement). Hence we can imagine that phenyl substituents of MG dye is still readily to rotate in the nanoparticles and thus the excess TFPB adsorption would not much contribute to strong rigidification of MG molecules. From a viewpoint of surface chemistry, PVP plays an important role in decreasing the size of the organic nanoparticles (or, in increasing the surface-to-volume ratio) through its surface adsorption.[22,39] In consideration with the fact that MG nanoparticles prepared at $\rho = 1$ with PVP (30–90 nm) had a (slightly) longer fluorescence average lifetime than those prepared without PVP (see Table 1), the polymer in contact with the nanoparticle surface would give an significant contribution to immobilizing the chromophoric MG molecules, bringing about the fluorescence enhancement. On this basis, we can reasonably conclude that the surface region of nanoparticles (including the surface-attached PVP) has greater rigidity compared to the inner region.

Conclusions

In summary, far-red fluorescent organic nanoparticles were synthesized via ion-association between malachite green (MG) cation and tetrakis(4-fluorophenyl)borate (TFPB) anion in the presence of a neutral stabilizing polymer PVP in water. The particle size could be tuned by adjusting the molar ratio of the loaded TFPB anion to the MG dye cation. Binding of MG with TFPB resulted in the prominent appearance of an absorption band that can be assigned to the dye H-aggregates. The fluorescence quantum yield as well as the fluorescence lifetime displayed a significant increase with a decrease in the nanoparticle size. In consideration with the fact that MG dye is known as a local viscosity probe that shows the rotational friction dependence of the fluorescence lifetime, the particle rigidity (environmental rigidity around MG in the nanoparticle) was strongly size dependent; the smaller the size of the organic nanoparticle became, the greater the particle rigidity inside. The presence of almost non-fluorescent H-aggregates still avoided enhancing the fluorescence quantum yield of the MG nanoparticles (ACQ; aggregation-caused quenching), so we developed a new way to prevent H-aggregation inside the MG nanoparticles by incorporation of photochemically inert phosphonium cations, which results in a 430-fold enhancement of its fluorescence yield. We believe organic nanoparticles synthesized on the basis of the ACG-suppressed methodology will provide a wide range of fluorescent probes for many biological and analytical

applications.

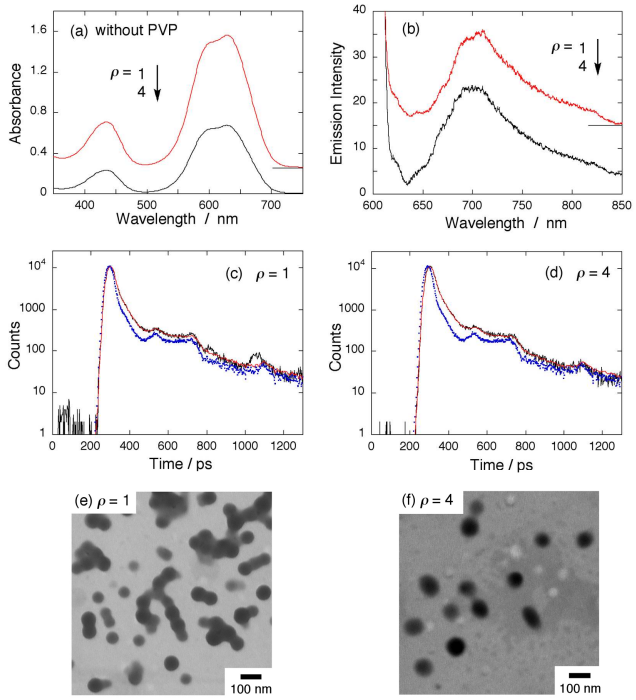

Fig. 7. (a) Absorption and (b) fluorescence spectra of MG nanoparticles prepared at $\rho = 1$ and 4 without using the PVP polymer. Spectra are offset by a constant (absorbance; 0.25 each, emission; 15 each) for clarity. (c) and (d) Fluorescence decay curves of MG nanoparticles prepared at $\rho = 1$ and 4, in the absence of PVP, in aqueous solution, respectively. (e) and (f) Typical STEM images of MG nanoparticles prepared at $\rho = 1$ and 4, in the absence of PVP, in aqueous solution, respectively.

Notes and references

[a] *Address, Graduate School of Material Science, University of Hyogo, 3-2-1 Koto, Kamigori-cho, Ako-gun, Hyogo 678-1297, Japan. Fax: 81-791-58-0161; E-mail: yao@sci.u-hyogo.ac.jp*

[b] *Address, Department of Chemistry, School of Science and Technology, Kwansei Gakuin University, 2-1 Gakuen, Sanda, Hyogo 669-1337, Japan*

† Electronic Supplementary Information (ESI) available: [time evolution of the solution-phase absorption spectra of MG nanoparticle samples synthesized in the presence of PVP, optimized structures of MG and 1:1 ion-pair adduct of MG–TFPB calculated at the DFT level, and fluorescence decay curve of MG in water]. See DOI: 10.1039/b000000x/

‡ (i) The width of IRF in this study warrants that lifetimes longer than ~8 ps are well-defined. The statistical error of lifetimes obtained in the present system would be at most ±3–6%.[40] (ii) In MG nanoparticles prepared in the presence of PVP, the lifetime of the third component (τ_3) obtained by tri-exponential analysis was always 2–3 ns, whereas bi-exponential analysis never gave a component with such a long lifetime. In other words, nanoparticles larger than 40–50 nm did not have the third component with a lifetime of 2–3 ns. This suggests that τ_3 should be determined by an asymptotic value of particle rigidity (or environmental rigidity around the MG molecules) that would be achieved when the nanoparticle diameter became smaller than 40–50 nm.

§ The fluorescence dymanics of MG depends here on both the particle regidity and energy transfer from monomer to the non-fluorescent H-aggregates. In the present case, despite an increase in the amount of H-aggregates at a high ρ value, the average fluorescence lifetime increased, suggesting that the energy transfer is unlikely to occur.

1 D. Ding, K. Li, Z. Zhu, K.-Y. Pu, Y. Hu, X. Jiang and B. Liu, *Nanoscale*, 2011, **3**, 1997.
2 R. Weissleder, *Nat. Biotechnol*., 2001, **19**, 316.
3 W. Qin, D. Ding, J. Liu, W. Z. Yuan, Y. Hu, B. Liu and B. Z. Tang, *Adv. Funct. Mater*., 2012, **22**, 771.
4 M. J. Baars and G. Patonay, *Anal. Chem*., 1999, **71**, 667.
5 B. L. Legendre Jr., D. L. Moberg, D. C. Williams and S. A. Soper, *J. Chromatogr. A*, 1997, **779**, 185.
6 S. Achilefu, *Technol. Cancer Res. Treat*., 2004, **3**, 393.
7 K. Kiyose, H. Kojima and T. Nagano, *Chem. Asian J*., 2008, **3**, 506.
8 A. B. Descalzo, H.-J. Xu, Z. Shen and K. Rurack, *Ann. N. Y. Acad. Sci*., 2008, **1130**, 164.
9 M. Bruchez Jr., M. Moronne, P. Gin, S. Weiss and A. P. Alivisatos, *Science*, 1998, **281**, 2013.
10 X. Shu, A. Royant, M. Z. Lin, T. A. Aguilera, V. Lev-Ram, P. A. Steinbach and R. Y. Tsien, *Science*, 2009, **324**, 804.
11 C. Loo, A. Lowery, N. Halas, J. West and R. Drezek, *Nano Lett*., 2005, **5**, 709.
12 C. Szent-Gyorgyi, B. F. Schmidt, Y. Creeger, G. W. Fisher, K. L. Zakel, S. Adler, J. A. Fitzpatrick, C. A. Woolford, Q. Yan, K. V. Vasilev, P. B. Berget, M. P. Bruchez, J. W. Jarvik and A. Waggoner, *Nat. Biotechnol*., 2008, **26**, 235.
13 J. R. Babendure, S. R. Adams and R. Y. Tsien, *J. Am. Chem. Soc*., 2003, **125**, 14716.
14 K. Li, W. Qin, D. Ding, N. Tomczak, J. Geng, R. Liu, J. Liu, X. Zhang, H. Liu, B. Liu and B. Z. Tang, *Sci. Reports*., 2013, **3**, 1150.
15 D. F. Duxbury, *Chem. Rev*., 1993, **93**, 381.
16 D. Ben-Amotz and C. B. Harris, *J. Chem. Phys*., 1987, **86**, 4856.
17 V. Sundström and T. Gillbro, *J. Chem. Phys*., 1984, **81**, 3463.
18 A. C. Bhasikuttan, A. V. Sapre and T. Okada, *J. Phys. Chem. A*, 2003, **107**, 3030.
19 A. Mokhtari, A. Chebira and J. Chesnoy, *J. Opt. Soc. Am. B*, 1990, **8**, 1551.
20 D. A. Cremers and M. W. Windsor, *Chem. Phys. Lett*., 1980, **71**, 27.
21 M. M. Martin, E. Breheret, F. Nesa and Y. H. Meyer, *Chem. Phys*., 1989, **130**, 279.
22 H. Yao, in *Advanced Fluorescence Reporters in Chemistry and Biology II, in Springer Series on Fluorescence*, ed. by A. P. Demchenko, Springer, Heidelberg, 2010, Vol. 9, 285–304.
23 H. Yao and K. Ashiba, *RSC Adv*., 2011, **1**, 834.
24 H. Yao and K. Ashiba, *ChemPhysChem*, 2012, **13**, 2703.
25 H. Yao and T. Enseki, *J. Photochem. Photobiol. A: Chem*., 2013, **271**, 124.
26 P. F. Aramendía, R. M. Negrí and E. S. Román, *J. Phys. Chem*., 1994, **98**, 3165.
27 A. Mandal and N. Tamai, *J. Phys. Chem. C*, 2008, **112**, 8244.
28 N. Tamai, M. Ishikawa, N. Kitamura and H. Masuhara, *Chem. Phys. Lett*., 1991, **184**, 398.
29 M. Ziólek, I. Tacchini, M. T. Martínez, X. Yang, L. Sund and A. Douhal, *Phys. Chem. Chem. Phys*., 2011, **13**, 4032–4044.
30 D. Grate and C. Wilson, *Proc. Natl. Acad. Sci. U.S.A*., 1999, **96**, 6131.
31 M. Kasha, *Physical Processes in Radiation Biology*, Academic Press: New York, 1964.
32 H. Yao, Y. Inoue, H. Ikeda, K. Nakatani, H.-B. Kim and N. Kitamura, *J. Phys. Chem*., 1996, **100**, 1494.
33 J. Mohanty and W. M. Nau, *Angew. Chem*., 2005, **117**, 3816 .
34 J. Y. Ye, T. Hattori, H. Nakatsuka, Y. Maruyama and M. Ishikawa, *Phys. Rev. B*, 1997, **56**, 5286.
35 R. Trebino and A. E. Siegman, *J. Chem. Phys*., 1983, **79**, 3621.
36 P. Fita, A. Punzi and E. Vauthey, *J. Phys. Chem. C*, 2009, **113**, 20705.
37 A. Nakayama and T. Taketsugu, *J. Phys. Chem. A*, 2011, **115**, 8808.
38 S. Rafiq, R. Yadav and P. Sen, *J. Phys. Chem. B*, 2010, **114**, 13988.
39 M. R. Böhmer, L. K. Koopal and R. Janssen, *Langmuir*, 1992, **8**, 2228.
40 N. Boens, W. Qin, N. Basarić, J. Hofkens, M. Ameloot, J. Pouget, J.-P. Lefèvre, B. Valeur, E. Gratton, M. vandeVen, N. D. Silva , Jr., Y. Engelborghs, K. Willaert, A. Sillen, G. Rumbles, D. Phillips, A. J. W. G. Visser, A. van Hoek, J. R. Lakowicz, H. Malak, I. Gryczynski, A.

G. Szabo, D. T. Krajcarski, N. Tamai, and Atsushi Miura, *Anal. Chem*., 2007, **79**, 2137.